

Testing the transverse field Ising model in LiHoF₄ using capacitive dilatometryJ. L. Dunn,^{1,2,*} C. Stahl,² A. J. Macdonald,² Kevin Liu,² Y. Reshitnyk,² W. Sim,² and R. W. Hill^{1,2}¹*GWPI, University of Waterloo, Waterloo, Ontario N2L 3G1, Canada*²*Department of Physics and Astronomy, University of Waterloo, Waterloo, Ontario N2L 3G1, Canada*

(Received 30 May 2010; published 24 September 2012)

Measurements of thermal expansion and magnetostriction on a single-crystal sample of the Ising ferromagnetic material, LiHoF₄, are presented. The strain is measured along the crystallographic *c* axis (the Ising direction) of the material and the magnetic field is applied transverse to this, in the *ab* plane. The data are used to extract critical fields and critical temperatures for the ferromagnetic transition, resulting in a phase diagram for this material. The measurements are strongly focused on the very low magnetic field regime, where previous magnetic susceptibility data show a discrepancy with theory based on the transverse field Ising model, although the previous experimental data density is very sparse. The results of this study generate a high-resolution magnetic phase line that is consistent with previous measurements and therefore confirm the discrepancy. These detailed measurements can be used to significantly constrain any future theoretical work which aims to explain the observed behavior.

DOI: [10.1103/PhysRevB.86.094428](https://doi.org/10.1103/PhysRevB.86.094428)

PACS number(s): 75.30.Kz, 65.40.De, 65.60.+a, 75.80.+q

I. INTRODUCTION

The study of quantum phase transitions is of considerable current interest in condensed matter physics.¹ The interest is motivated, on the one hand, by the drive to understand and potentially harness all things quantum mechanical and, on the other, by the realization that many, as yet poorly understood, phenomena may be caused by quantum fluctuations associated with an underlying quantum critical point. One important example is the high-temperature cuprate superconductors, where much of the unusual physics could possibly be ascribed to a quantum critical point lying underneath the dome of superconductivity in the doping phase diagram.² However, such an example is an extremely complicated problem and our interest in understanding quantum phase transitions may be better served by studying a more tractable quantum critical system.

One of the simplest models to exhibit a quantum phase transition is the transverse field Ising model. Here, a magnetic field applied transverse to the magnetic Ising direction is used to suppress the magnetic ordering temperature to 0. The suppression occurs because the transverse field couples the two Ising states and allows quantum mechanical tunneling from one state to the other. As the transverse field is increased, quantum mechanical fluctuations associated with the tunneling process become large enough that the Ising order is destroyed and the system enters a spin-polarized state known as a quantum paramagnet. Because the phase transition occurs at zero temperature and is driven by quantum rather than thermal fluctuations, it is consequently termed a quantum phase transition. A schematic phase diagram is shown in Fig. 1.

The application of this model to real magnetic systems will be stringent test of our ability to model and describe the effect of quantum fluctuations on physical properties in the simplest case. From this benchmark we can then explore further complexities that will occur, for example, in strongly correlated systems.

The topic of this paper is the transverse field Ising model as applied to the ferromagnetic material LiHoF₄. As described in Sec. II, this material has been studied in this context before from both an experimental and a theoretical standpoint. Our

goal here is to concentrate on a particular regime of the transverse field phase diagram, where there is a long-standing discrepancy between theory and experiment. This is in the high-temperature, low-field regime, where theory predicts a more rapid suppression of the ferromagnetic transition temperature than has been observed experimentally. However, prior to this work, the quantity of experimental data points in this regime was very low and a high-resolution study was required to establish the extent of the discrepancy from the experimental side.

In this paper, we report thermal expansion and magnetostriction measurements on a single crystal of LiHoF₄ in the presence of a magnetic field applied perpendicular to the direction of the ferromagnetic ordering. The results of our measurements are used to extract a transition temperature as a function of the magnetic field and construct a high-resolution phase line for this system which we compare with theory based on the transverse field Ising model.

Our results show that, even in this simple case of quantum criticality, it is not clear that our understanding is as complete as we might expect. Consistent with earlier experimental work, there is a clear discrepancy between the theoretical implementation of the model and the measured experimental data. Surprisingly, it exists not where quantum fluctuations are large, but in the high-temperature, low-field regime, where thermal fluctuations are dominant and the quantum fluctuations are smallest. Whether this is truly a lack of knowledge about the interplay between thermal and quantum fluctuations or a shortcoming of LiHoF₄ as a model system is an open question.

The rest of this paper is organized as follows: in Sec. II, we review the material LiHoF₄ and the theoretical and experimental work that has gone before in the context of the transverse field Ising model; in Sec. III, the technique, measurement apparatus, and method of data analysis are discussed; Sec. IV presents the measured linear thermal expansion and linear magnetostriction coefficients of LiHoF₄ and the methods used to determine critical points; and, finally, in Sec. V, we present discussion and conclusions stemming from the results of this investigation into the transverse field

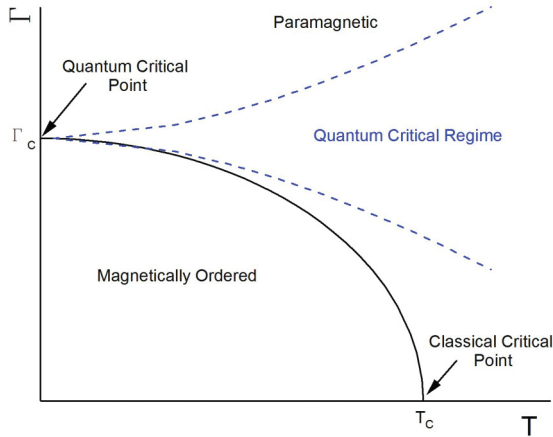


FIG. 1. (Color online) A schematic phase diagram of the transverse field Ising model where T is the temperature and Γ is the effective transverse field parameter. The solid line separates the magnetically ordered phase from the paramagnetic phase.

Ising model as it applies to LiHoF₄ and other model Ising systems.

II. PREVIOUS THEORETICAL AND EXPERIMENTAL WORK

LiHoF₄ has a face-centered tetragonal crystal structure. The lattice parameters are reported to be $a = a' = 5.175 \text{ \AA}$ and $c = 10.75 \text{ \AA}$.³ The magnetic behavior is due to the Ho³⁺ ions with a $4f^{10}$ electronic structure. Application of Hund's rules dictates a free ion spin state 5I_8 that is 17-fold degenerate. Situated in the crystal structure of LiHoF₄, the degeneracy is split by the presence of the Li⁺ and F⁻ ions, which generate a large crystal field. The resulting ground state is a non-Kramers doublet with spins pointing parallel and antiparallel to the crystallographic c axis. This is separated from the first excited state, a singlet, which has an energy that is approximately 11 K above the ground-state energy.⁴ The consequence of this magnetic energy level scheme is that, at low temperatures with respect to the energy of the first excited state, the system has Ising anisotropy.

Experimentally, LiHoF₄ has been found to order ferromagnetically at the Curie temperature, $T_c = 1.53 \text{ K}$.⁵⁻⁸ The small ionic radius of the Ho³⁺ ions reduces the effect of exchange coupling in comparison to dipolar coupling. Fitting data from either magnetic susceptibility measurements⁵ or specific heat measurements⁷ gives a dominant dipolar coupling that is ferromagnetic with an antiferromagnetic exchange coupling that is smaller by a factor of approximately 2. With the ground state established as an Ising ferromagnet, applying a magnetic field transverse to the Ising direction (c axis) should, in principle, realize one of the simplest theoretical models to describe a quantum phase transition, namely, the transverse field Ising model.

The Hamiltonian for the transverse field Ising model, originally proposed by de Gennes,⁹ can be expressed as^{10,11}

$$H = -\frac{1}{2} \sum_{i>j} J_{ij} \sigma_i^z \sigma_j^z + \Gamma \sum_i \sigma_i^x. \quad (1)$$

Here J_{ij} are coupling constants between spins, $\sigma_i^{x,y,z}$ are Pauli operators, and Γ is the effective transverse field parameter, which represents the mixing of the two Ising states in the presence of the physical transverse magnetic field. For $\Gamma \neq 0$, quantum mechanical fluctuations in the Ising order occur even at zero temperature. Increasing the fluctuations by increasing the transverse field eventually leads to a disordering of the magnetically ordered phase at a critical value of $\Gamma = \Gamma_c$. This is the quantum critical point.

The application of a magnetic field transverse to the Ising (easy) axis of LiHoF₄ splits the ground-state doublet and introduces quantum mechanical tunneling between the Ising states of the Ho³⁺ ions in the presence of the crystalline electric field. The associated quantum fluctuations lead to a suppression of the Curie temperature with increasing field, culminating in a quantum phase transition when the transition temperature is suppressed to 0.

Bitko *et al.*¹² were the first to report the phase line of the ferromagnetic state in LiHoF₄ in a transverse magnetic field using measurements of magnetic susceptibility down to millikelvin temperatures. The Curie temperature was observed to be suppressed to zero temperature at a critical magnetic field of 4.2 T. A successful theoretical fit to the data was presented using mean field theory with two adjustable parameters; the transverse component of the Landé g -factor tensor and the effective longitudinal spin-spin coupling strength. These terms rescale the effect of the transverse magnetic field and temperature, respectively.

To gain further insight and include the effect of fluctuations, there have been several theoretical studies of LiHoF₄ starting from a full microscopic Hamiltonian. The full Hamiltonian includes crystal field effects, magnetic dipolar and exchange coupling, and hyperfine coupling. Such a complicated Hamiltonian is a long way from the simple expression for the transverse field Ising model given in Eq. (1). Consequently, the full microscopic Hamiltonian must be recast as an effective spin-1/2 Ising model to which an effective transverse magnetic field is applied.

Chakraborty *et al.*¹³ were the first to try this approach to produce a superior theoretical model and use quantum Monte Carlo simulations to calculate the transverse magnetic field phase diagram. The treatment included the effects of quantum fluctuations and the domain structure of the ferromagnetic state. Parameters in the theory were fixed, where possible, by results from spectroscopic¹⁴ and susceptibility⁴ measurements, leaving one adjustable parameter as the magnitude of the antiferromagnetic Heisenberg exchange coupling. This parameter is necessary to obtain the measured zero-field value of the ferromagnetic ordering temperature, which is lower by some 25% than the quantum Monte Carlo value in the absence of this coupling. Using this approach, a phase line was computed that agreed well with the data, particularly in the low-temperature limit where quantum fluctuations are significant. Nonetheless, a discrepancy with the data close to the zero-field transition was apparent and reported as reflecting the potential uncertainties in the crystal field parameters for LiHoF₄.¹³

Further theoretical work on the transverse field Ising model as it relates to LiHoF₄ followed Rønnow *et al.*¹⁵ That study addressed neutron scattering spectra¹⁶ as well as the phase

line measured earlier.¹² The critical points determined from neutron scattering experiments lacked close agreement at a low transverse field compared to previous susceptibility work.¹² For the theoretical calculation, the crystal-field parameters were derived from spectroscopic measurements^{14,17,18} on Ho-doped LiYF_4 and agreed closely with previously determined values.⁴ As in the Chakraborty work,¹³ the computed phase line overestimated the rate of suppression of the ferromagnetic state at very low transverse fields. However, given that different crystal field parameters are used, but still lead to a discrepancy between theory and experiment similar to that seen earlier, it is unlikely that this is the source of the problem.

Most recently, a substantial theoretical effort by Tabei *et al.*¹⁰ has been reported that, in particular, attempts to resolve the differences between the theoretical phase line and experiment at low transverse fields.^{13,15} Using the fact that in this regime the quantum fluctuations are small, they were introduced perturbatively into a classical Hamiltonian. The calculation then proceeded using classical Monte Carlo techniques that were both significantly different and simpler to implement than their quantum Monte Carlo counterparts. The possible sources of discrepancy were separated into ones which were computational in nature and ones that resulted from inadequacies in the model Hamiltonian. The authors concluded that the discrepancy was not of computational origin, nor did it stem from uncertainties in crystal-field parameters. Consequently, it was most likely due to shortcomings of the model Hamiltonian [Eq. (1)] used. Furthermore, they also made the suggestion that the experimental determination of the phase diagram should be revisited. This provided substantial motivation for the study reported here.

As outlined above, there have been several attempts to improve the theoretical understanding of the phase diagram of LiHoF_4 , while little has been done to repeat the experimental measurement of the phase diagram, particularly in the low-field region where the data density is very low. Here we report a detailed experimental study of the phase line using thermal expansion and magnetostriction measurements. We focus exclusively on the high-temperature–low-field regime, where there are markedly few data points from the original experimental investigation¹² and where the theory is most challenged. Our results show a good agreement with the existing experimental data where there is overlap. Moreover, we provide a high-resolution phase line that will tightly constrain and guide the further theoretical work that will be required to explain the physical behavior.

III. APPARATUS AND EXPERIMENTAL METHOD

Previous experimental investigations have made use of magnetic susceptibility,¹² neutron scattering,¹⁶ and specific heat⁸ (zero-field only) to determine critical points in the phase diagram of LiHoF_4 . For the study reported here, capacitive dilatometry has been used to measure the linear thermal expansion and linear magnetostriction measured along the c axis (or [001] axis) of a commercial LiHoF_4 sample.¹⁹ In the remainder of this article, the terms thermal expansion and magnetostriction should be interpreted as the linear measurement.

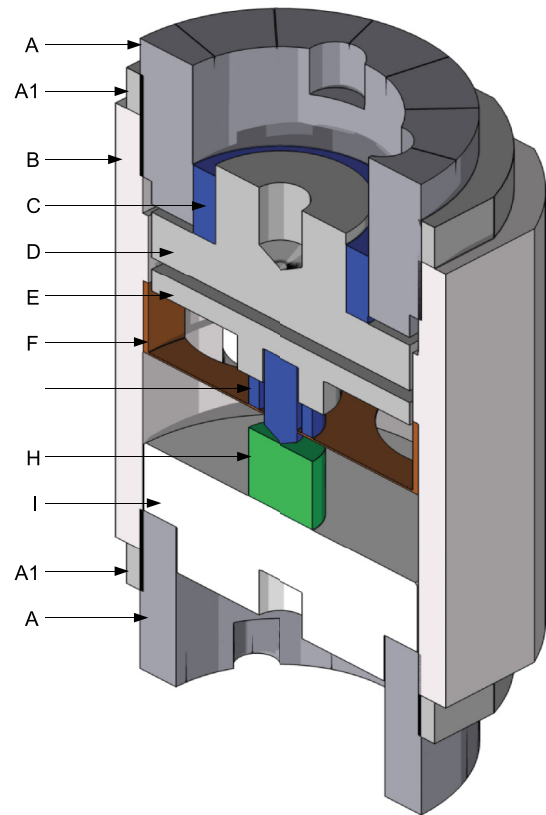


FIG. 2. (Color online) A sketch of the dilatometer used in this work. Two A304 stainless steel positioners at the top and bottom (labeled A) thread into a silver shell (labeled B). The positioners and the shell are threaded at 80 turns/in., or 3.14 turns/mm. Positioners are held in place using A304 stainless steel nuts (A1). The fixed capacitor plate (D) is mounted inside the upper positioner and electrically isolated with a sapphire washer (C). The capacitance between the upper (D) and the lower (E) capacitor plates is determined by the plate separation (and the plate area). The lower capacitor plate (E) is fixed to a beryllium-copper spring (F) using a sapphire pin and washer (G). The sample (H) is mounted to a sample base (I), and the lower positioner (A) is used to adjust the position of the sample base (I) and, consequently, press the sample (H) against the BeCu spring (F). When assembled, the dilatometer is between 23 and 27 mm long, depending on the length of the sample. The outer cross section of the shell is a 15-mm square; an inner circular bore contains the other components shown. All inner components are circular and concentric with the inner bore of the shell. The area of the circular capacitor plates is approximately 108 mm^2 .

The capacitive dilatometer is shown schematically in Fig. 2. The principle of operation is very similar to that for other devices published in the literature (see, e.g., Refs. 20 and 21). Essentially, one plate of a parallel-plate capacitor is fixed, while the other is attached to the top of a sample. A change in the length of the sample results in a change in the separation of the capacitor plates and, consequently, a change in the capacitance. Measuring the capacitance as a function of the temperature or magnetic field allows the linear thermal expansion or magnetostriction coefficient to be computed.

The device used here has been designed to have flexibility in accommodating sample size, spring deflection (and,

consequently, force on the sample), and plate separation (which influences the device sensitivity). This is achieved by having both the fixed capacitor plate and the sample base adjustable using positioners that move on a very fine pitch thread (3.14 turns/mm) in the shell of the capacitor.

Referring to Fig. 2, the shell (B), capacitor plates (D, E) and sample base (I) are machined from 99.995% pure silver to ensure that the device is nonmagnetic and has a high thermal conductivity and that there is no large nuclear heat capacity at low temperatures and high magnetic fields (compared to copper). The spring (F) that keeps the movable capacitor plate (E) in contact with the sample is machined from beryllium-copper and then hardened to ensure that it keeps its flexibility at low temperatures. The capacitor plates are electrically isolated from the shell, spring, and sample using sapphire spacers (C, G). Where necessary, a small amount of Stycast epoxy is used to join parts of the dilatometer together. However, the design is such that the epoxy layer is always transverse to the direction of capacitor plate displacement so as to reduce any effect of this material on the measurable thermal expansion of the cell. The position of the fixed capacitor plate and the sample base relative to the shell are adjusted using two A304 stainless steel positioners (A), which are threaded into the shell. Once the desired position is achieved, they are tightened in place using stainless steel lock nuts (A1).

The sample (H) is thermally linked to a sample base (I) using a silver paint.²² A small amount of vacuum grease is applied around the sample-spring contact in order to reduce any transverse displacement of the ferromagnetic sample in an applied field (see Sec. IV D). Thermal stability of the sample is monitored by an uncalibrated Cernox CX-1030 resistance thermometer that is fastened directly to the bottom of the sample base. Uniaxial pressure applied to the sample was less than 5 MPa for the investigation presented here.

The small amount of Stycast epoxy and creep of screw threads will add a small nonrepeatable contribution to the measured thermal expansion. As shown in the measurement of the cell effect in Fig. 3, this contribution is approximately 2 orders of magnitude smaller than the magnitude of the thermal expansion of LiHoF_4 . The nonrepeatable contribution from screws and epoxy does not affect the determination of the critical points in LiHoF_4 .

A more detailed description of the design, manufacture, and testing of the capacitive dilatometer is provided in the M.Sc. thesis of J. Dunn.²³

The LiHoF_4 sample is taken from a commercially produced single crystal.¹⁹ It is shaped as a roughly semicircular plate and is approximately 1 mm thick, 5.5 mm tall, and about 3.5 mm at its widest point. The easy [001] axis of the LiHoF_4 sample was determined to within $\pm 1^\circ$ using a commercial Laue diffraction setup, and the ends of the crystal subsequently polished to be orthogonal to this easy axis within 2.5° . When placed in the dilatometer, length changes along the [001] axis were measured as the temperature and magnetic field were varied. The effects of torque applied to the sample were investigated by changing the polarity of the applied field; while there was an observed qualitative change in the thermal expansion coefficient, the determination of critical points from the measured data was not affected. These tests are presented in Sec. IV D.

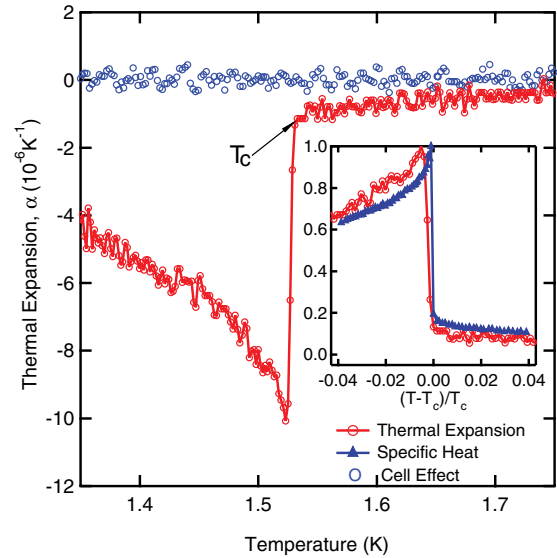


FIG. 3. (Color online) Zero-field measurement of the linear thermal expansion coefficient, α , of LiHoF_4 measured along [001] and the cell effect as a function of temperature. The critical temperature, T_c is indicated, being the first deviation from the paramagnetic state. Inset: Thermal expansion coefficient and specific heat measurements from Ref. 8, both normalized to their peak value as a function of reduced temperature.

The dilatometer is clamped to the 1 K pot of a pumped ^4He cryostat, which is used to cool the sample mounted in the dilatometer to approximately 1 K. The clamp allows the dilatometer to be oriented such that the cylindrical axis of the dilatometer and, consequently, the [001] axis of the sample are perpendicular to the magnetic field direction when the cryostat is inserted into the vertical bore of the superconducting magnet. Combined with the sample polishing and mounting, this arrangement sets up the transverse field configuration with an estimated overall accuracy of $\pm 5^\circ$.

The temperature is controlled using a Lakeshore 331 temperature controller and measured by a calibrated Cernox CX-1030 resistor located on the cold stage of the pumped ^4He cryostat. For measurements of thermal expansion, an experimental trial consists of a temperature sweep through the region of interest (≈ 1.2 to 1.8 K) at a rate of 7.5 mK/min. Cernox resistors have a low magnetoresistance that must be accounted for in order to assign the correct temperature when the magnetic field is applied, particularly given the small shifts in the transition temperature that are measured at very low transverse fields. The correction is applied by interpolating the magnetoresistance data from Brandt *et al.*²⁴ For magnetostriction measurements, the temperature is controlled to within ± 1 mK, while the magnetic field is swept at a rate of 0.2 T/min. The magnetoresistance of the temperature sensor leads to a small nonmonotonic variation in the temperature as the magnetic field sweep proceeds. We estimate this to be less than $\pm 5\%$ of the temperature over the entire magnetic field range.

Capacitance was measured using a commercial Andeen-Hagerling 2500A capacitance bridge, with a resolution of 10^{-7} pF, which equates to a dilation of 0.002 \AA at 17 pF. The measured capacitance is converted to capacitor plate

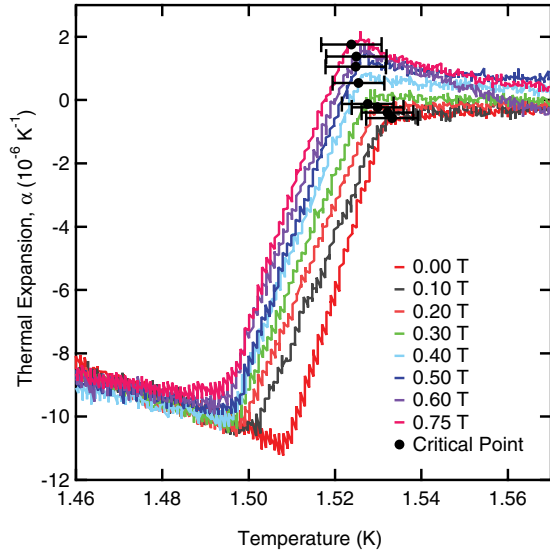


FIG. 4. (Color online) Measurement of the linear thermal expansion coefficient, α , for LiHoF₄ along [001] up to an applied transverse field of $H = 0.75$ T. The critical temperature at each field is indicated.

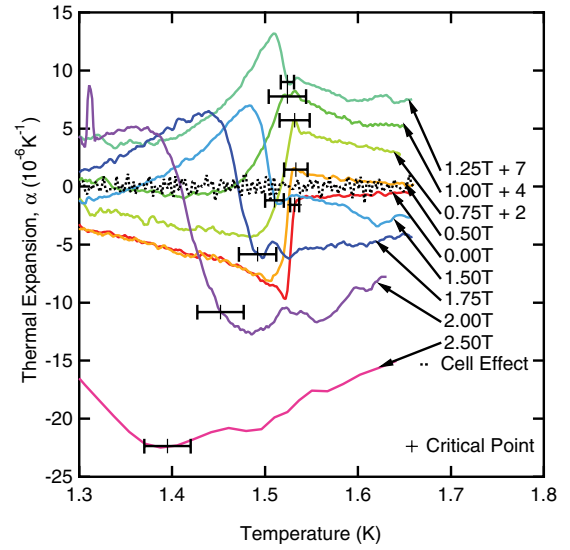


FIG. 5. (Color online) Measurement of the linear thermal expansion coefficient, α , for LiHoF₄ along [001] up to an applied transverse field of $H = 2.5$ T. The critical temperature at each field is indicated. The legend indicates any offset in units of 10^{-6} K^{-1} .

separation, D , using an expression for a tilted plate capacitor,²⁵

$$D = \frac{\epsilon_0 A}{C} \left[1 + \left(\frac{C}{C_{\max}} \right)^2 \right], \quad (2)$$

where ϵ_0 is the permittivity of free space, A is the effective capacitor plate area, C_{\max} is the maximum measured capacitance before the capacitor plates short, and C is the measured capacitance. While the capacitor plates are nominally parallel, using Eq. (2) allows for slight deviations from this ideal situation. Prior to beginning a measurement, the maximum capacitance (C_{\max} ; typically ≈ 50 pF) is measured. This is the measured capacitance just before the plates touch and electrically short (leading to $C = 0$ pF). Once typical operating conditions are taken into account, length changes greater than 0.2 \AA can be resolved. A measured change in the capacitor plate spacing is directly related to a change in the sample length, $dD = -dL$. However, the computed length change will include the effect of the dilatometer cell as well as the LiHoF₄ sample. To isolate the behavior of the sample from the measured change in capacitance requires a measurement of the cell with a silver sample. This quantity is known as the cell effect (see Fig. 3). Ultimately, the quantity of interest is the thermal expansion coefficient, $\alpha(T)$, which is the normalized rate of change of length with temperature. The relation between the measured thermal expansion coefficient and the thermal expansion coefficient of LiHoF₄ is²⁶

$$\alpha_{\text{LiHoF}_4} = \frac{1}{L} \frac{dL}{dT} \Big|_{\text{Cell+LiHoF}_4} - \frac{1}{L} \frac{dL}{dT} \Big|_{\text{Cell+Ag}+\alpha_{\text{Ag}}}, \quad (3)$$

where α_{Ag} is the thermal expansion coefficient of silver²⁷ and L is the length of the sample. An analogous expression for magnetostriction can be derived, replacing temperature with applied transverse field.²³

IV. RESULTS

A. Thermal expansion

1. Zero field

In Fig. 3, the linear thermal expansion of LiHoF₄ measured along the c axis is plotted in the absence of any magnetic field. The transition from the paramagnetic to the ferromagnetic state as the temperature is lowered results in a sudden jump in the thermal expansion coefficient. To be consistent with previous experimental¹² and theoretical work,¹³ we define the critical temperature, T_c , as the first deviation from the behavior in the paramagnetic state as the temperature is decreased. This point is determined from the intersection of a polynomial fit to the temperature dependence of the thermal expansion above the transition and a linear fit to the steepest section of the thermal expansion during the transition (increasing the order of either fit made no appreciable difference). The error in this determination was estimated by varying the range of the fitted curves near the critical region by up to ± 0.05 K (10% of the temperature range) and observing the range of T_c 's that result.

Using the above analysis, the transition temperature in zero field is $T_c = 1.532 \pm 0.005$ K. In the inset to Fig. 3, we plot the thermal expansion data and high-resolution specific heat data.⁸ One can relate the thermal expansion coefficient (α) to the specific heat (C_v) through the Grüneisen parameter (γ) and the bulk modulus (B): $\alpha(T) = (\gamma/3B)C_v(T)$. Assuming that the Grüneisen parameter and the bulk modulus are temperature independent, it is apparent that the discontinuities observed in specific heat measurements should be reproduced in a thermal expansion measurement. To aid close comparison, the thermal expansion data are inverted and both measurements are normalized to their peak values while being plotted against the reduced temperature with respect to their individual transition temperatures. The qualitative agreement is excellent (as shown in the inset in Fig. 3). Quantitatively, there is a small discrepancy between the absolute values of the

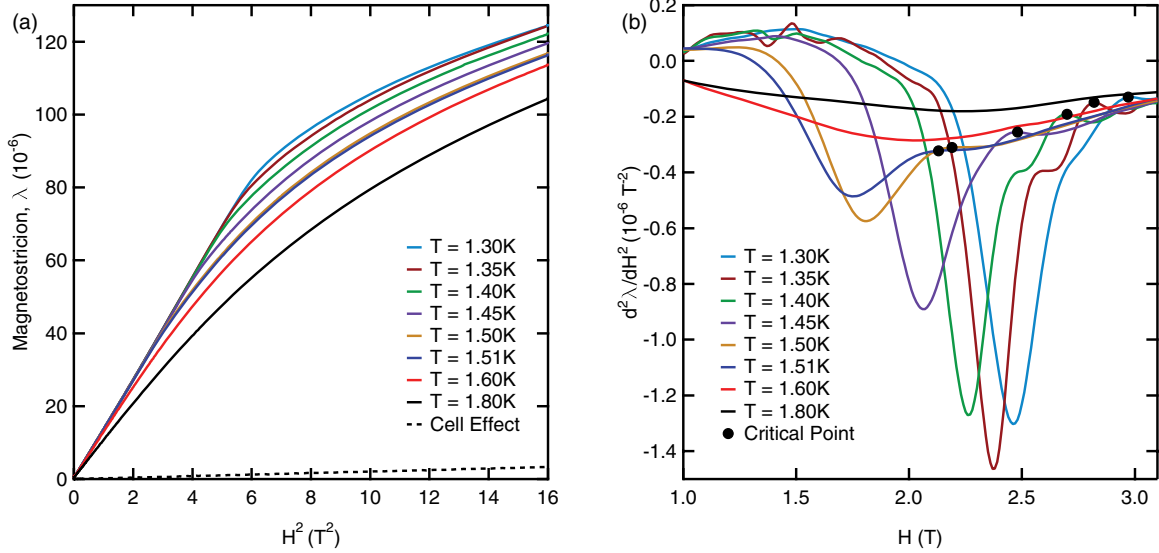


FIG. 6. (Color online) (a) Magnetic-field-induced strain ($\Delta L/L$) as a function of the square of the transverse field, H^2 . (b) Second derivative of the strain with respect to the magnetic field versus the transverse magnetic field. The critical points are taken as the field at which the derivative deviates from the featureless behavior measured in the paramagnetic phase ($T > 1.53$ K).

transition temperatures (1.532 ± 0.005 and 1.5384 K), and the transition width is larger by 4 mK in the thermal expansion measurements. Both effects can reasonably be attributed to the swept temperature method that was used in this experiment.

2. Transverse magnetic field

The magnetic field is applied perpendicular to the c axis. The tetragonal structure of LiHoF_4 means that the response will be isotropic with respect to the field direction in the plane perpendicular to the c axis. However, the irregular shape of the sample means that any demagnetisation correction to the applied field can be minimized by orienting the thin face perpendicular to the field. We identify this as the minimum demagnetization direction and it is at an angle of 15° to the a axis. The demagnetization correction factor is discussed more fully in Sec. IV C.

The evolution of the temperature dependence of the linear thermal expansion in a low transverse field (≤ 0.75 T) is shown in Fig. 4. The effect of the small transverse field on the transition from the paramagnetic to the ferromagnetic phase is small, serving only to reduce the temperature of the phase transition, with minimal effect on the qualitative shape. The transition temperature is extracted from these data in the same manner as for the zero-field measurement and is also plotted in Fig. 4.

The thermal expansion transition over a broader range of transverse magnetic fields is shown in Fig. 5. Select curves at each field have been offset for clarity, as indicated in the legend. The data now exhibit a broadening of the transition from the paramagnetic to the ferromagnetic state as the magnetic field is increased. There is also a qualitative change in the shape of the transition as the field is increased. For magnetic fields up to $H = 1$ T (see also Fig. 4), the thermal expansion coefficient decreases as the ferromagnetic state is entered. For fields above this value the opposite change is observed and the expansion coefficient increases.

As in the zero-field measurement, the transition temperature for all measurements is defined as the first deviation from the monotonic behavior that is considered the paramagnetic phase. The same analysis as described above is used to extract a transition temperature at each magnetic field. As the transition width broadens, this increases the uncertainty of the determination of the transition temperature T_c as indicated by the error bar (Fig. 5).

B. Magnetostriction

Magnetostriction is the change in volume of a material in response to a magnetic field. In Fig. 6(a), the normalized change in length, $\lambda = \Delta L/L$, versus the transverse magnetic field squared is plotted. At low fields, the change in length has the appropriate H^2 form consistent with a magnetic-field-independent susceptibility²⁸ as measured by Bitko *et al.*¹² At a higher field, the magnetostriction begins to saturate as the system becomes polarized and the magnetization becomes saturated. In between these two extremes the data evolve smoothly at all temperatures regardless of whether the system changes from ferromagnetic to paramagnetic or remains entirely in the paramagnetic phase. In spite of the absence of any distinct feature at the phase transition, there is a distinct qualitative difference between the two types of curves, with the data where the sample undergoes a ferromagnetic transition exhibiting a more pronounced shoulder.

The very broad response of the dilation with magnetic field makes extracting a critical field, H_c , more difficult than for the thermal expansion measurements. First, we note that the cell effect measured with a silver sample is very small and featureless [see Fig 6(a)]. To extract a critical field, the second derivative of the change in length with magnetic field is used. This is plotted in Fig. 6(b). For data entirely in the paramagnetic phase ($T = 1.60$ and 1.80 K), the second derivative is a smooth featureless curve. As the temperature is lowered and the material magnetically orders on lowering

the magnetic field, a distinct peak develops in the data. Consistent with our definition for the critical temperature in the thermal expansion results, we take the initial deviation of the response from the smooth variation as the field is lowered to be the critical field. These are the data points plotted on the respective curves in the figure. Although this critical field value is nominally at a fixed temperature, the actual temperature is complicated by the magnetoresistance of the temperature sensor. Having established the critical field, the actual temperature is determined by applying a magnetoresistance correction for the Cernox thermometer as described earlier. This is a small correction, amounting to no more than $\pm 5\%$ at all fields and temperatures.

C. Demagnetization effects

The irregular shape of the sample means that the demagnetization factor due to uncompensated spins on the surface of the material is difficult to calculate. However, we can assess the impact of the demagnetization effect on our results by orienting either the semicircular face or the thin edge of the crystal perpendicular to the transverse field. Since they are orthogonal and the crystal structure is tetragonal, both directions are 15° from the crystallographic a axis. These two experimental orientations represent the maximum and the minimum demagnetization factor for this particular sample. In the following we estimate the difference in the magnitude of the demagnetization factor between the two orientations.

The demagnetization correction can be written as $H_{\text{Internal}} = H_{\text{Applied}} - GM$, where H is either the internal or the applied magnetic field, G is the demagnetization factor resulting from the crystal geometry, and M is the sample magnetization. To a first approximation, the difference between H_{Internal} and H_{Applied} will be determined wholly by G , when the only experimental change is the orientation of the crystal and we assume the magnetization to be the same in each situation. For an anisotropic sample, an appreciable demagnetization correction would effectively shift the determined critical temperature at some applied field, through an anisotropic response of H_{Internal} with respect to the applied field. Beleggia *et al.*²⁹ proposed a scheme for magnetostatic mapping of shapes to equivalent ellipsoids whose demagnetization factors can be more easily calculated. Following this work, we can estimate the demagnetization factors of the LiHoF₄ sample used in this work by a rectangular prism with dimensions $L_x = 1$ mm, $L_y = 2.1$ mm, and $L_z = 5.5$ mm.

Using the Mathematica code provided in the above reference, we find the demagnetization factors $G_x = G_{\text{max}} = 7.55$, $G_y = G_{\text{min}} = 1.68$, and $G_z = -0.32$. Thus, the correction for the maximum demagnetization orientation will be approximately 4.5 times larger than in the minimum demagnetization orientation. By repeating the same experiments using these two sample orientations, we can compare demagnetization corrections. As expected, in all orientations, the observed zero-field transitions are identical and occur at $T_c = 1.532 \pm 0.005$ K.

Figure 7 shows the results of such an investigation at $H = 2.5$ T. As can be seen, a striking feature of this test is the qualitative difference in the temperature dependence of the thermal expansion between orientations. The transition tem-

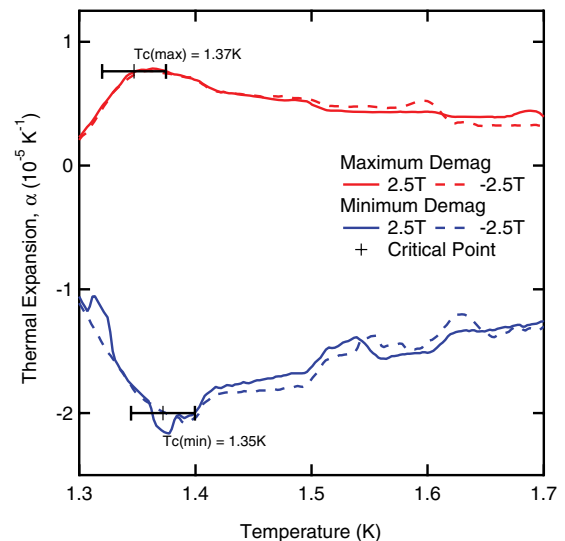


FIG. 7. (Color online) Measurement of α for LiHoF₄ at ± 2.5 T in the maximum [upper (red) lines] and minimum [lower (blue) lines] demagnetization orientations. Crosses show the calculated critical temperatures [$T_{c,\text{max}(\text{min})}$] along with an associated error bar. The dashed red (blue) line shows the thermal expansion for the identical sample orientation but with the field direction reversed.

perature which is extracted is $T_c(\text{max}) = 1.37 \pm 0.03$ K and $T_c(\text{min}) = 1.35 \pm 0.03$ K for each orientation, as shown by the crosses in the figure. Consequently, despite the difference in the demagnetization factor of almost 5, there is only a small difference in the internal field H_{Internal} for each orientation and so the transition temperature shifts by an amount which is less than our uncertainty in each value. This suggests that the demagnetization correction will lead to changes in T_c that are at most within our current error estimates.

The preceding analysis assumes that the sample is single domain. Calculation of the demagnetization factor is a far more complicated issue in the presence of domains.^{30,31} Nonetheless, even in the presence of a magnetic domain structure, we would still anticipate an orientation dependence to the demagnetization factor for this sample and the empirical evidence from this study is that this correction is small. Theoretical analysis of the domain structure in LiHoF₄ has been carried out by Biltmo and Henelius.³² We speculate that differences in the domain structure that could occur for each orientation may explain the qualitative orientational difference in the signal that is measured. Moreover, the evolution of the domain structure with the applied field may also explain the qualitative trends in the thermal expansion data shown in Fig. 5. A better understanding of the microscopic origin of the thermal expansion coefficient and the behavior of domains in the region of the transition would be required to explain this observation.

D. Torque effects

The potential misalignment of a ferromagnetic sample in a transverse magnetic field may lead to a torque on the sample, which, if the sample were to rotate or bend, could lead to a signal indistinguishable from thermal expansion or magnetostriction. To minimize the displacement of the LiHoF₄ sample within the dilatometer, the sample was fastened at both

ends. The bond at the sample holder was made using silver paint, while the bond at the spring was made using vacuum grease. In both cases, a small amount of the bonding agent was used around the sample such that it would not contribute to thermal expansion measurements.

Nevertheless, in order to verify that any torque applied to LiHoF_4 was not distorting our ability to measure the phase transition, thermal expansion was measured in positive and negative transverse fields, while in both the minimum and the maximum demagnetization orientations. As shown in Fig. 7, the measured thermal expansion for both field directions is identical. Consequently we conclude that any rotation or bending of the sample does not hinder our ability to determine critical points in thermal expansion measurements of LiHoF_4 .

V. DISCUSSION AND CONCLUSIONS

Combining the ferromagnetic-to-paramagnetic critical temperatures from thermal expansion measurements with critical fields from magnetostriction measurements produces the phase diagram shown in Fig. 8. The increasing error bars with applied field reflect the broadening of the transition region and, consequently, the associated difficulty in assigning a transition temperature rather than a loss of precision in our technique. Also plotted are the critical points from earlier magnetic susceptibility¹² and neutron scattering¹⁶ work and from the latest numerical simulations.¹⁰ There is excellent agreement between the experimental data from our technique and the magnetic susceptibility, thereby confirming the discrepancy with the current theoretical simulations. Qualitatively, what appears to occur is that when a transverse field is applied to LiHoF_4 there is initially no change to the ferromagnetic phase transition temperature. It is only when the field rises above 1 T, which is approximately 25% of the field required to completely suppress the ferromagnetism at zero temperature, that the transition temperature starts to be suppressed. The origin of this imperviousness to the transverse field is unknown and would appear to be an aspect of the physics that is not captured by the transverse field Ising model [Eq. (1)] used to describe LiHoF_4 in numerical simulations.^{10,13,15} What is now important to assess is whether these results reveal a generic lack of understanding of the impact of quantum fluctuations at finite temperature or the simplistic nature of the transverse field model as applied to LiHoF_4 .

One aspect of physics that is specific to LiHoF_4 is the effect of magnetoelastic coupling on the antiferromagnetic or quadrupolar exchange parameters as discussed in earlier theoretical studies.^{10,15} These couplings compete with the ferromagnetic coupling and clearly affect the transition temperature. For example, the magnitude of the antiferromagnetic exchange is used as an adjustable parameter to generate the correct zero-field transition temperature in the theoretical models.^{10,13,15} Introducing a field dependence to this exchange parameter such that it becomes weaker with magnetic field would qualitatively correct the theoretical phase line in an appropriate way to match the data. An interesting possibility would be that if the exchange decreased sufficiently quickly with magnetic field, the magnetic ordering could be re-entrant. However, this possibility is ruled out by our high-resolution study, which clearly shows there is no re-entrant behavior.

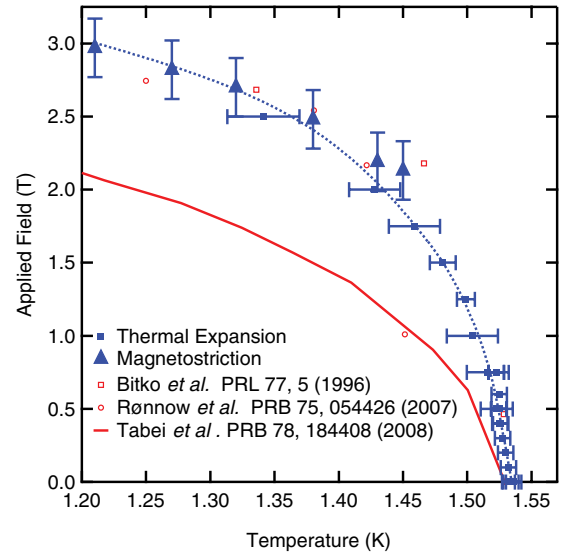


FIG. 8. (Color online) Transverse field versus temperature phase diagram of LiHoF_4 , as measured in this study using thermal expansion (squares) and magnetostriction (circles) data. Also plotted is previous experimental^{12,16} and theoretical Monte Carlo¹⁰ work. The dotted line is a guide for the eye.

On the theoretical side, Rønnow *et al.*¹⁵ estimated that a strain $\epsilon_{13} \sim 10^{-4}$ would be required to produce a noticeable effect in the transition temperature due to the quadrupolar interactions. Our measurements of magnetostriction are only along the c axis (ϵ_{33}) so we are unable to address this issue directly. However, the overall magnitude of the magnetostriction measured in this study is $\Delta l/l \sim 10^{-6}$. Consequently, unless the magnitude of the in-plane magnetostriction is dramatically different (i.e., 2 orders of magnitude larger), it is unlikely that this could lead to a significant restoration of the critical temperature to compensate for the reducing effect of the quantum fluctuations. Further studies of magnetostriction to lower temperatures including measurements along the a axis would be required to provide a more complete picture. A qualitative change in magnetostrictive behavior between measurements shown here at temperatures very close to $T_c(0)$ and those at lower temperatures, where agreement with theory is much better, would be illuminating.

On a related point, we note that the magnetic field scale of 1 T also signifies a qualitative change in the behavior of the transition in thermal expansion between the paramagnetic and the ferromagnetic state, as shown in Fig. 5. In the absence of a detailed microscopic theory describing the features of the transition, we are not able to assess whether this is a related phenomena or merely coincidental. As already discussed, an experimental investigation of domain wall motion to complement existing theoretical work³² would be invaluable. Careful analysis of the evolution of the transition in any other technique may also provide additional insight.

Very recently, identical physics has been explored in an Fe_8 single molecular magnet.³³ This material orders ferromagnetically at $T_c = 0.6$ K. The magnetic phase line has been measured as a function of the applied transverse field using magnetic susceptibility. At very low fields, one observes behavior remarkably similar to that measured for LiHoF_4 in

that the rate of T_c suppression is initially very slow. This argues for a more generic explanation for this phenomenon than using properties specific to LiHoF_4 .

Finally, investigation of other Ising systems, for example, $\text{Ho}(\text{OH})_3$ and $\text{Dy}(\text{OH})_3$, as proposed by Stasiak *et al.*,³⁴ could determine if this discrepancy between the theoretical model and the experimental work is particular to this material or is a generic feature of the effect of a transverse field on Ising magnetism in real systems.

In conclusion, we have used measurements of thermal expansion and magnetostriction to map the phase diagram of LiHoF_4 in a transverse magnetic field at temperatures close to the zero-field classical phase transition where quantum fluctuations are small. The resultant phase line separating the paramagnetic phase from the ferromagnetic phase is in agreement with earlier experimental studies¹² and disagrees with

current theoretical results based on the transverse field Ising model.^{10,13} The crucial issue now is whether the disagreement pertains to details of the LiHoF_4 system or whether it is a generic feature signifying a lack of understanding of the effect of quantum fluctuations at finite temperature.

ACKNOWLEDGMENTS

We acknowledge J. Kycia for supplying the LiHoF_4 sample used in this study. Thanks go to M. J. P. Gingras, J. Kycia, J. Quilliam, P. Stasiak, and A. Tabei for helpful discussion. We would also like to acknowledge the skill of Mike Lang and the assistance of Harman Vander Heide in the construction of the dilatometer. Financial support was provided by NSERC, the University of Waterloo, and Oxford Instruments PLC.

*Corresponding author: jl2dunn@uwaterloo.ca

¹S. Sachdev, ed., *Quantum Phase Transitions* (Cambridge University Press, Cambridge, 2009).

²N. P. Butch, K. Jin, K. Kirshenbaum, R. L. Greene, and J. Paglione, *Proc. Natl. Acad. Sci. USA* **109**, 8440 (2012).

³C. Keller and H. Schmutz, *J. Inorg. Nucl. Chem.* **27**, 900 (1965).

⁴P. E. Hansen, T. Johansson, and R. Nevald, *Phys. Rev. B* **12**, 5315 (1975).

⁵A. H. Cooke, D. A. Jones, J. F. A. Silva, and M. R. Wells, *J. Phys. C: Solid State Phys.* **8**, 4083 (1975).

⁶P. Beauvillain, J.-P. Renard, I. Laursen, and P. J. Walker, *Phys. Rev. B* **18**, 3360 (1978).

⁷G. Mennenga, L. J. de Jongh, and W. J. Huiskamp, *J. Mag. Mag. Mat.* **44**, 59 (1985).

⁸J. Nikkel and B. Ellman, *Phys. Rev. B* **64**, 214420 (2001).

⁹P. D. Gennes, *Solid State Commun.* **1**, 132 (1963).

¹⁰S. M. A. Tabei, M. J. P. Gingras, Y. J. Kao, and T. Yavors'kii, *Phys. Rev. B* **78**, 184408 (2008).

¹¹M. Schechter and P. C. E. Stamp, *Phys. Rev. B* **78**, 054438 (2008).

¹²D. Bitko, T. F. Rosenbaum, and G. Aeppli, *Phys. Rev. Lett.* **77**, 940 (1996).

¹³P. B. Chakraborty, P. Henelius, H. Kjønsberg, A. W. Sandvik, and S. M. Girvin, *Phys. Rev. B* **70**, 144411 (2004).

¹⁴H. P. Christensen, *Phys. Rev. B* **19**, 6564 (1979).

¹⁵H. M. Rønnow, J. Jensen, R. Parthasarathy, G. Aeppli, T. F. Rosenbaum, D. F. McMorrow, and C. Kraemer, *Phys. Rev. B* **75**, 054426 (2007).

¹⁶H. M. Rønnow, R. Parthasarathy, J. Jensen, G. Aeppli, T. F. Rosenbaum, and D. F. McMorrow, *Science* **308**, 392 (2005).

¹⁷S. Salaün, M. T. Fornoni, A. Bulou, M. Rousseau, P. Simon, and J. Y. Gesland, *J. Phys.: Condens. Matter* **9**, 6941 (1997).

¹⁸J. Magariño, J. Tuchendler, P. Beauvillain, and I. Laursen, *Phys. Rev. B* **21**, 18 (1980).

¹⁹Purchased from TYDEX, J.S.Co., St. Petersburg, Russia.

²⁰H. Matsui, S. Yanagida, and T. Goto, *Jpn. J. Appl. Phys.* **31**, 2941 (1992).

²¹H. Subrahmanyam and S. Subramanyam, *Jpn. J. Appl. Phys.* **27**, 5 (1986).

²²Purchased from Dupont Canada; product no. 4929N.

²³J. Dunn, Master's thesis, University of Waterloo, 2010; <http://hdl.handle.net/10012/5609>.

²⁴B. L. Brandt, D. W. Liu, and L. G. Rubin, *Rev. Sci. Instrum.* **70**, 104 (1999).

²⁵C. A. Swenson, *Thermal Expansion of Solids* (ASM International, Materials Park, OH, 1998), p. 207.

²⁶G. M. Schmiedeshoff, *Rev. Sci. Instrum.* **77**, 123907 (2006).

²⁷D. R. Smith and F. R. Fickett, *J. Res. Natl. Inst. Stand. Technol.* **100**, 119 (1995).

²⁸B. Chandrasekhar and E. Fawcett, *Adv. Phys.* **20**, 775 (1971).

²⁹M. Beleggia, M. D. Graef, and Y. T. Millev, *J. Phys. D: Appl. Phys.* **39**, 891 (2006).

³⁰L. Neel, *Adv. Phys.* **4**, 191 (1955).

³¹D. J. Dunlop, *Geophys. Res. Lett.* **10**, 79 (1983).

³²A. Biltmo and P. Henelius, *Europhys. Lett.* **87**, 27007 (2009).

³³E. Burzuri, F. Luis, B. Barbara, R. Ballou, E. Ressouche, O. Montero, J. Campo, and S. Maegawa, *Phys. Rev. Lett.* **107**, 097203 (2011).

³⁴P. Stasiak and M. J. P. Gingras, *Phys. Rev. B* **78**, 224412 (2008).